

---

# A SHAPE-NEWTON METHOD FOR FREE-BOUNDARY PROBLEMS SUBJECT TO THE BERNOULLI BOUNDARY CONDITION

---

Yiyun Fan, John Billingham, and Kristoffer van der Zee  
School of Mathematical Sciences  
University of Nottingham

## ABSTRACT

We develop a shape-Newton method for solving generic free-boundary problems where one of the free-boundary conditions is governed by the Bernoulli equation. The Newton-like scheme is developed by employing shape derivatives in the weak forms, which allows us to update the position of the free surface and the potential on the free boundary by solving a boundary-value problem at each iteration. To validate the effectiveness of the approach, we apply the scheme to solve a problem involving the flow over a submerged triangular obstacle.

## 1 Introduction

Free boundary problems have many applications in fluid mechanics, such as open-channel flow, fluid/solid interaction and hydrodynamics. The difficulty in solving such problems arises since the geometry of the domain needs to be determined together with other variables in this problem. A simplified but important model problem is the Bernoulli free-boundary problem, which considers the (linear) Dirichlet and Neumann boundary condition on the free boundary [1, 2]. This is not to be confused with the Bernoulli equation, which is the pressure boundary condition in the irrotational fluid mechanics, and which we will also study in this paper. The nonlinearity of the Bernoulli equation poses an additional challenge to numerical algorithms.

There are several computational approaches to this class of problems. The first is to solve the boundary value problem with the single free-boundary condition for the field variables on a fixed approximated domain and update the free surface derived from the remaining free boundary condition, which is not included in the boundary value problem. These fixed-point type methods are called trial methods, which converge linearly and cannot always find a solution. The details can be found, for example, in [2, 3, 4].

The second approach is to formulate a shape optimization problem to improve the convergence rate. This method aims to construct a boundary-value problem as the state problem with one free-boundary condition and formulate a cost function with the remaining free-boundary condition. However, this approach requires gradient information and is applied to a particular free-boundary problem. The formulation and application of shape optimization to free boundary problems can be found in, e.g. [5, 6, 7, 8, 9, 10].

The third approach is linearising the whole system and applying a Newton-type method. One linearisation method, called domain-map linearisation, requires us to transform the free-boundary problem to an equivalent boundary value problem on a fixed domain and then linearise the transformed problem concerning the reference domain [11, 12]. An alternative way to linearise the free-boundary problem is to apply shape calculus to the current geometry [13, 14]. Kärkkäinen and Tiihonen used this technique to solve two different free-boundary problems: a particular Bernoulli free-boundary problem [15] and a stationary free boundary problem [16]. The application to a more general Bernoulli free-boundary problem has been investigated in [17] by considering the whole problem in one weak form and reformulating the problem with a curvature-dependant boundary condition to analyse with  $C^1$  continuous free boundary. The use of shape calculus and a Newton-type method is called the shape-Newton method.

In the current work, we extend the shape-Newton method to a more generic free-boundary problem by considering the Bernoulli boundary condition on the free surface. We also recall the method for the Bernoulli free-boundary problem, which has a Dirichlet boundary condition on the free boundary. In addition, we consider Robin boundary conditions

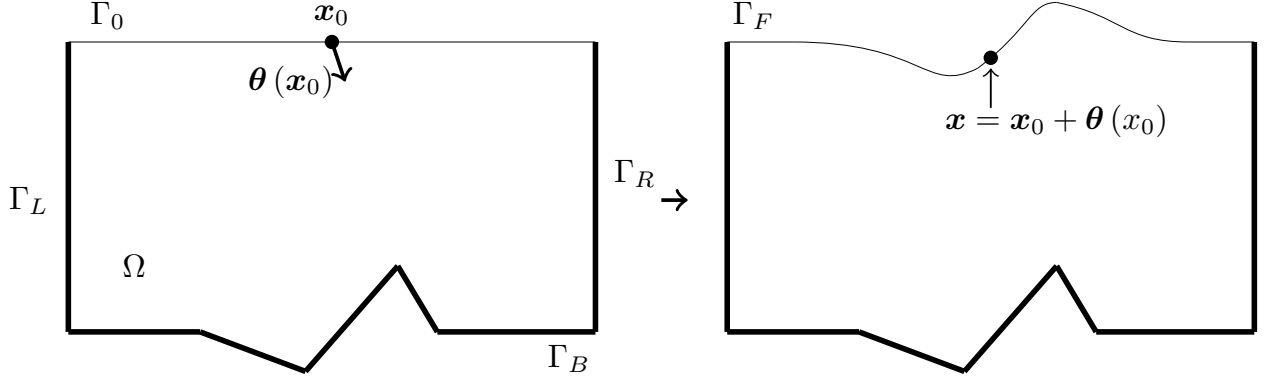


Figure 1: The sketch of the parametrization of the free boundary  $\Gamma_F$  by the displacement  $\theta(x_0)$  with respect to the reference boundary  $\Gamma_0$ .

on the fixed boundary. Similar to Kärkkäinen and Tiihonen, the problem will be set up in terms of two weak forms: one derived from the boundary value problem with the Neumann boundary condition over the current domain, and the other from the remaining free boundary condition (Dirichlet condition or Bernoulli condition). The linearisation for the Dirichlet free-boundary problem is known. However, the linearisation for the Bernoulli equation has not been derived before: we obtain a surprisingly simple expression for the shape derivative, which involves the normal derivative of the velocity squared ( $|\nabla^2 \phi|$ ); see section 5.3. We will show a numerical experiment involving open channel flow over a submerged triangle [18]. The shape-Newton method converges superlinearly, and the results agree well with the exact solutions or the results in the reference paper.

The contents of this paper are arranged as follows. We will first introduce the model problem either with the Dirichlet boundary condition or the Bernoulli equation on the free boundary in Section 2. In Section 3, we will derive the weak form for both problems. Then, we will introduce some basic concepts about shape derivatives in Section 4 and the linearisation by applying Hadamard shape derivatives for the free-boundary problem follows in Section 5. In Section 6, we will illustrate the Newton-like and coupled schemes. The numerical experiments will be shown in Section 7, following the conclusions in Section 8.

## 2 Free-boundary Problem with Bernoulli or Dirichlet free-boundary condition

We investigate the free boundary problem with either the Bernoulli condition or the Dirichlet condition on the free boundary. The Bernoulli condition is commonly used when considering steady, incompressible, and inviscid flow, but it is nonlinear, making the boundary value problem more challenging to solve. Hence, the Bernoulli equation can be simplified as the Dirichlet boundary condition such that the nonlinearity in the free-boundary condition is not included in this problem. To be more general, the boundary conditions on the fixed boundaries are Robin boundary conditions.

### 2.1 Free-boundary Problem With Bernoulli Condition

The free-boundary problem with a Bernoulli condition can be abstracted as seeking an unknown domain  $\Omega \subset \mathbb{R}^N$  and a corresponding scalar function  $\phi : \Omega \rightarrow \mathbb{R}$ . The boundary  $\partial\Omega$  contains a free boundary  $\Gamma_F$ , a left boundary  $\Gamma_L$  for input flow, a right boundary  $\Gamma_R$  for output flow, and the bed  $\Gamma_B$ . Figure 1 is an example of the domain and the parametrization of the free boundary  $\Gamma_F$ , where the bed boundary can have any shape. The vertical displacement of the free boundary is denoted as  $\eta(x)$ . The problem can be presented as

$$-\Delta \phi = f, \quad \text{in } \Omega, \quad (1)$$

$$\partial_{\mathbf{n}} \phi = 0, \quad \text{on } \Gamma_F, \quad (2)$$

$$\partial_{\mathbf{n}} \phi + \omega \phi = g + \omega h, \quad \text{on } \partial\Omega \setminus \Gamma_F, \quad (3)$$

$$a |\nabla \phi|^2 + b \eta + c = 0, \quad \text{on } \Gamma_F, \quad (4)$$

where  $\partial_{\mathbf{n}}(\cdot) = \mathbf{n} \cdot \nabla(\cdot)$  is the normal derivative with  $\mathbf{n}$  being the unit normal vector to the boundary pointing out the domain. The condition (4) with real-valued constants  $a, b$ , and  $c$  represents the Bernoulli condition. We have Robin boundary conditions on  $\partial\Omega \setminus \Gamma_F$  where  $\omega, g$  and  $h$  are the boundary data. Thus we can approximate either a Neumann or Dirichlet-type condition depending on the values of  $\omega$ . The Neumann boundary condition, obtained when  $\omega = 0$ , usually represents the kinematic condition, where the perpendicular fluid velocity is zero on the free or solid boundary.

On the other hand, choosing  $\omega$  to be extremely large yields the approximated Dirichlet boundary condition  $\phi = h$ . Furthermore, it is possible to impose mixed boundary conditions by choosing various values of  $\omega$  on different parts of the boundaries (i.e.  $\Gamma_L$ ,  $\Gamma_R$  and  $\Gamma_B$ ). Sufficiently  $\mathcal{C}^1$ -smooth data  $f$ ,  $g$  and  $h$  allow us to find a nontrivial solution pair  $(\Gamma_F, \phi)$ .

By introducing a vector field  $\boldsymbol{\theta} : \Gamma_0 \rightarrow \mathbb{R}^N$ , the displacement of the free boundary with respect to the referenced boundary  $\Gamma_0$  can be defined as

$$\Gamma_F := \{\mathbf{x} \in \mathbb{R}^N | \mathbf{x} = \mathbf{x}_0 + \boldsymbol{\theta}(\mathbf{x}_0), \forall \mathbf{x}_0 \in \Gamma_0\}, \quad (5)$$

to parametrize the domain  $\Omega$  and the free boundary  $\Gamma_F$ , as shown in Figure 1. This allows us to write the problem (1)-(4) in terms of the pair  $(\boldsymbol{\theta}, \phi)$ . Considering  $\eta(x)$  in (4) denoted as the  $y$ -component of  $\theta$ , the problem (1)-(4) can alternatively be resolved using the pair  $(\eta, \phi)$  for fixed values of  $x$ .

## 2.2 Free-boundary Problem with Dirichlet Boundary Condition

A more straightforward model problem is introduced by replacing the Bernoulli condition with the Dirichlet condition on the free boundary. The boundary-value problem is now linear and easier to solve. The abstract problem is

$$-\Delta\phi = f, \quad \text{in } \Omega, \quad (6)$$

$$\partial_{\mathbf{n}}\phi = 0, \quad \text{on } \Gamma_F, \quad (7)$$

$$\partial_{\mathbf{n}}\phi + \omega\phi = g + \omega h, \quad \text{on } \partial\Omega \setminus \Gamma_F, \quad (8)$$

$$\phi = h, \quad \text{on } \Gamma_F, \quad (9)$$

where  $g \leq 0$  for input flow and  $h$  is assumed to be sufficiently smooth on  $\mathbb{R}^N$ .

By choosing  $\omega \rightarrow \infty$  for Dirichlet boundary conditions on  $\partial\Omega \setminus \Gamma_F$ , this problem is quite similar to a classical free-boundary problem for an ideal fluid, called Bernoulli free-boundary problem [2].

## 3 The Weak Form

We will first find the weak forms of both free-boundary problems to apply shape-calculus techniques to linearise this problem. Let  $\Gamma_D$  represent the boundary  $\partial\Omega \setminus \Gamma_F$  with Dirichlet boundary conditions and  $x_L$  represent the  $x$ -component of the left node on the free boundary  $\Gamma_F$ , we introduce the test functions  $v \in V := \{v \in \mathcal{C}^1(\Omega) | v = 0 \text{ on } \Gamma_D\}$  and  $w \in W := \{w \in \mathcal{C}^1(\Gamma) | w = 0 \text{ on } x_L\}$ . If no Dirichlet boundary conditions are given on any part of the boundary  $\partial\Omega \setminus \Gamma_F$ , then the test function  $v$  satisfies  $v \in V := \mathcal{C}^1$ .

Since the only difference between the two free-boundary problems in Section 2 is the Bernoulli condition and the Dirichlet condition on the free boundary, the first weak form in the domain  $\Omega$  is the same in both situations. It can be obtained by integrating the multiplication of the Laplacian equation ((1) or (6)) and the test function  $v$  over  $\Omega$ , then applying the Green's formula with the Robin boundary conditions on  $\partial\Omega \setminus \Gamma_F$  and Neumann boundary condition on  $\Gamma_F$ , yielding

$$\mathcal{R}_1((\boldsymbol{\theta}, \phi); v) = 0, \quad \forall v \in V, \quad (10)$$

where the semilinear form  $\mathcal{R}_1((\boldsymbol{\theta}, \phi); v)$  is defined as

$$\begin{aligned} \mathcal{R}_1((\boldsymbol{\theta}, \phi); v) &= \int_{\Omega} \Delta\phi \cdot v d\Omega - \int_{\Omega} f v d\Omega, \\ &= \int_{\Omega} \nabla\phi \cdot \nabla v d\Omega - \int_{\partial\Omega \setminus \Gamma_F} g v ds - \int_{\Omega} f v d\Omega. \end{aligned} \quad (11)$$

However, when  $\omega \rightarrow \infty$  yields the Dirichlet boundary condition on the fixed boundary, we will replace the weak form on the fixed boundary with the strong form  $\phi = h$  instead to enforce  $\phi$  to satisfy the boundary condition.

The second weak form is different on the free boundary, which can be derived by multiplying with test function  $w$  and integrating over  $\Gamma_F$ ,

$$\mathcal{R}_2((\boldsymbol{\theta}, \phi); w) = 0, \quad \forall w \in W, \quad (12)$$

with the definition of the semilinear form  $\mathcal{R}_2((\boldsymbol{\theta}, \phi); w)$  as

$$\mathcal{R}_2((\boldsymbol{\theta}, \phi); w) = \int_{\Gamma_F} (\text{B.C}) w d\Gamma, \quad (13)$$

where (B.C) can either be the left hand side of Bernoulli condition (4) or Dirichlet condition (9).

## 4 Shape Derivatives

The linearisation of  $\mathcal{R}_1((\boldsymbol{\theta}, \phi); v)$  and  $\mathcal{R}_2((\boldsymbol{\theta}, \phi); w)$  needs the differentiation of the weak forms with respect to the geometry, where the geometry itself is treated as a variable. Thus the shape derivatives are applied to find the differentiation defined in a fixed domain, which requires some appropriate smoothness assumptions.

The weak forms (11) and (13) contain domain integrals  $\int_{\Omega} (\cdot) d\Omega$  and boundary integrals  $\int_{\Gamma_F} (\cdot) d\Gamma$ . The shape derivatives for a domain integral and a boundary integral can be obtained by applying the Hadamard formula [13, 14] as

**Theorem 4.1.** (Shape derivative of domain integral) Suppose  $\phi \in W^{1,1}(\mathbb{R}^N)$  and  $\Omega$  is an open and bounded domain; we have the domain integral

$$J(\Omega) = \int_{\Omega} \phi d\Omega.$$

If  $\Gamma$  is the boundary of  $\Omega$  of class  $C^1$ , then its shape derivative with respect to the perturbation  $\delta\boldsymbol{\theta} \in C_0^1(\mathbb{R}^N; \mathbb{R}^N)$  is given by

$$\langle dJ(\Omega), \delta\boldsymbol{\theta} \rangle = \int_{\Gamma} \phi \delta\boldsymbol{\theta} \cdot \mathbf{n} d\Gamma,$$

where  $\mathbf{n}$  denotes the outward normal derivative to  $\Omega$ .

**Theorem 4.2.** (Shape derivative of boundary integral) Suppose  $\phi \in W^{2,1}(\mathbb{R}^N)$  and  $\Omega$  is an open and bounded domain with the boundary  $\Gamma$  of class  $C^{1,1}$ , we have the boundary integral

$$J(\Gamma) = \int_{\Gamma} \phi d\Gamma.$$

Then its shape derivative with respect to the perturbation  $\delta\boldsymbol{\theta} \in C_0^1(\mathbb{R}^N; \mathbb{R}^N)$  is given by

$$\langle dJ(\Gamma), \delta\boldsymbol{\theta} \rangle = \int_{\Gamma} (\partial_{\mathbf{n}}\phi + \kappa\phi) \delta\boldsymbol{\theta} \cdot \mathbf{n} d\Omega,$$

where  $\mathbf{n}$  denotes the normal vector to  $\Gamma$  and  $\kappa$  is the curvature of  $\Gamma$ .

In the above theorems,  $\delta\boldsymbol{\theta}$  is defined as

$$\delta\boldsymbol{\theta} = \delta\boldsymbol{\theta}(\mathbf{x}_0), \quad \text{with } \mathbf{x}_0 + \delta\boldsymbol{\theta}(\mathbf{x}_0) = \mathbf{x} \in \Gamma_F, \quad \text{and } \mathbf{x}_0 \in \Gamma_0,$$

where  $\Gamma_0$  is the reference domain.

## 5 Linearisation

The linearisation of  $\mathcal{R}_1((\boldsymbol{\theta}, u); v)$  and  $\mathcal{R}_2((\boldsymbol{\theta}, \phi); w)$  at an approximation pair  $(\hat{\boldsymbol{\theta}}, \hat{\phi})$  close to the exact solutions can be derived from the partial derivative of the weak forms with respect to  $\phi$  and  $\boldsymbol{\theta}$ . We assume that  $\hat{\phi}$  is any approximation satisfying the boundary conditions on  $\partial\Omega \setminus \Gamma_F$  that lives in the approximate domain  $\hat{\Omega}$  with the free boundary  $\hat{\Gamma}$  induced by the approximation  $\hat{\boldsymbol{\theta}}$ . The  $y$ -component of  $\hat{\boldsymbol{\theta}}$  is denoted as  $\hat{\eta}$ .

The Gâteaux derivative at  $\hat{\phi}$  in the direction  $\delta\phi$  and the linearisation for the Dirichlet boundary condition is relatively standard, similar to [17], while the approximation of the linearisation for Bernoulli condition is surprisingly elegant and straightforward.

### 5.1 Linearisation of $\mathcal{R}_1$

The Gâteaux derivative at  $\hat{\phi}$  in the direction  $\delta\phi$  can be evaluated as

$$\begin{aligned} \langle \partial_{\phi} \mathcal{R}_1((\hat{\boldsymbol{\theta}}, \hat{\phi}); v), \delta\phi \rangle &= \lim_{t \rightarrow 0} \frac{\mathcal{R}_1((\hat{\boldsymbol{\theta}}, \hat{\phi} + t\delta\phi); v) - \mathcal{R}_1((\hat{\boldsymbol{\theta}}, \hat{\phi}); v)}{t} \\ &= \int_{\hat{\Omega}} \nabla \delta\phi \cdot \nabla v d\Omega. \end{aligned} \quad (14)$$

Then the linearisation with respect to  $\boldsymbol{\theta}$  can be obtained by applying Hadamard formulas from Theorem 4.1 to (11) which yields

$$\langle \partial_{\boldsymbol{\theta}} \mathcal{R}_1((\hat{\boldsymbol{\theta}}, \hat{\phi}); v), \delta\boldsymbol{\theta} \rangle = \int_{\hat{\Gamma}} \nabla \hat{\phi} \cdot \nabla v \delta\boldsymbol{\theta} \cdot \mathbf{n} d\Gamma - \int_{\hat{\Gamma}} f v \delta\boldsymbol{\theta} \cdot \mathbf{n} d\Gamma. \quad (15)$$

The tangential gradient  $\nabla_\Gamma$  and tangential divergence  $\text{div}_\Gamma$  are defined as

$$\nabla_\Gamma(\cdot) = \nabla(\cdot) - \partial_n(\cdot)\mathbf{n}, \quad \text{div}_\Gamma = \text{div}(\cdot) - \partial_n(\cdot)\mathbf{n}. \quad (16)$$

By substituting (16) into (15) and applying the tangential Green's identity [13, 14], (15) can be approximated as

$$\begin{aligned} \langle \partial_\theta \mathcal{R}_1((\hat{\theta}, \hat{\phi}); v), \delta\theta \rangle &= \int_{\hat{\Gamma}} (\nabla_\Gamma \hat{\phi} \cdot \nabla_\Gamma v + \partial_n \hat{\phi} \partial_n v) \delta\theta \cdot \mathbf{n} d\Gamma - \int_{\hat{\Gamma}} f v \delta\theta \cdot \mathbf{n} d\Gamma \\ &\approx - \int_{\hat{\Gamma}} \text{div}_\Gamma (\delta\theta \cdot \mathbf{n} \nabla_\Gamma \hat{\phi}) v d\Omega - \int_{\hat{\Gamma}} f v \delta\theta \cdot \mathbf{n} d\Gamma \\ &\approx - \int_{\hat{\Gamma}} \text{div}_\Gamma (\delta\theta \cdot \mathbf{n} \nabla \hat{\phi}) v d\Omega - \int_{\hat{\Gamma}} f v \delta\theta \cdot \mathbf{n} d\Gamma. \end{aligned} \quad (17)$$

Due to the Neumann boundary condition (2) (or (7)),  $\partial_n \hat{\phi}$  is very small, and the related term is neglected in the second and third steps.

## 5.2 Linearisation of $\mathcal{R}_2$ with Dirichlet condition

Considering the Dirichlet boundary condition, we have

$$\mathcal{R}_2((\theta, \phi); w) = \int_{\Gamma_F} (\phi - h) w d\Gamma. \quad (18)$$

Similar to the linearisation of  $\mathcal{R}_1$  with respect to  $\phi$ , it is very straightforward to evaluate the Gâteaux derivative at  $\phi$  in the direction  $\delta\phi$ ,

$$\langle \partial_\theta \mathcal{R}_2((\hat{\theta}, \hat{\phi}); w), \delta\phi \rangle = \int_{\hat{\Gamma}} \delta\phi w d\Gamma. \quad (19)$$

Then by using the Hadamard formula on the boundary integral (18), we have the shape linearisation

$$\begin{aligned} \langle \partial_\theta \mathcal{R}_2((\hat{\theta}, \hat{\phi}); v), \delta\theta \rangle &= \int_{\hat{\Gamma}} (\partial_n + \kappa) [(\hat{\phi} - h) w] \delta\theta \cdot \mathbf{n} d\Gamma, \\ &= \int_{\hat{\Gamma}} [\partial_n (\hat{\phi} - h) w + (\hat{\phi} - h) \partial_n w + \kappa (\hat{\phi} - h) w] \delta\theta \cdot \mathbf{n} d\Gamma. \end{aligned} \quad (20)$$

Using the Dirichlet condition (9) and Neumann condition (7) on the free boundary, we can neglect the  $(\phi - h)$ -term and  $(\partial_n \phi)$ -term in (20). We then have the approximation

$$\langle \partial_\theta \mathcal{R}_2((\hat{\theta}, \hat{\phi}); v), \delta\theta \rangle \approx - \int_{\hat{\Gamma}} (\partial_n h) w \delta\theta \cdot \mathbf{n} d\Gamma. \quad (21)$$

## 5.3 Linearisation of $\mathcal{R}_2$ with Bernoulli condition

Substituting the Bernoulli condition (4) into the weak form (13), we have

$$\mathcal{R}_2((\theta, \phi); w) = \int_{\Gamma_F} (a |\nabla \phi|^2 + b\eta + c) w d\Gamma. \quad (22)$$

The linearisation in terms of  $\phi$  at approximation  $\hat{\phi}$  is

$$\langle \partial_\theta \mathcal{R}_2((\hat{\theta}, \hat{\phi}); w), \delta\phi \rangle = \int_{\hat{\Gamma}} 2a \nabla \hat{\phi} \cdot \nabla \delta\phi w d\Gamma. \quad (23)$$

To find the Gâteaux derivative with respect to  $\theta$  at  $\hat{\theta}$ , applying Hadamard formula yields

$$\begin{aligned} \langle \partial_\theta \mathcal{R}_2((\hat{\theta}, \hat{\phi}); v), \delta\theta \rangle &= \int_{\hat{\Gamma}} (\partial_n + \kappa) \left[ (a |\nabla \hat{\phi}|^2 + b\hat{\eta} + c) w \right] \delta\theta \cdot \mathbf{n} d\Gamma, \\ &= \int_{\hat{\Gamma}} \left( a \partial_n (|\nabla \hat{\phi}|^2) + b n_y \right) w \delta\theta \cdot \mathbf{n} d\Gamma \\ &\quad + \int_{\hat{\Gamma}} (a |\nabla \hat{\phi}|^2 + b\hat{\eta} + c) \partial_n w \delta\theta \cdot \mathbf{n} d\Gamma \\ &\quad + \int_{\hat{\Gamma}} \kappa (a |\nabla \hat{\phi}|^2 + b\hat{\eta} + c) w \delta\theta \cdot \mathbf{n} d\Gamma, \end{aligned} \quad (24)$$

where  $n_y$  is the  $y$ -coordinate of the unit normal vector  $\mathbf{n}$ . Since  $\hat{\eta}$  is the  $y$ -component of  $\hat{\theta}$ , we can evaluate  $\partial_{\mathbf{n}}\hat{\eta} = \partial_{\mathbf{n}}y = \begin{pmatrix} 0 \\ 1 \end{pmatrix} \cdot \begin{pmatrix} n_x \\ n_y \end{pmatrix} = n_y$ .

According to the Bernoulli condition (4),  $a \left| \nabla \hat{\phi} \right|^2 + b\hat{\eta} + c \rightarrow 0$  and can be neglected, thus the approximation is

$$\left\langle \partial_{\theta} \mathcal{R}_2 \left( \left( \hat{\theta}, \hat{\phi} \right); v \right), \delta \theta \right\rangle \approx \int_{\hat{\Gamma}} \left( a \partial_{\mathbf{n}} \left( \left| \nabla \hat{\phi} \right|^2 \right) + b n_y \right) w \delta \theta \cdot \mathbf{n} d\Gamma \quad (25)$$

Given  $\hat{\theta} = (x, \hat{\eta}(x))$ , we have the unit normal vector  $\mathbf{n} = \frac{1}{\sqrt{1+\hat{\eta}_x^2}} (-\hat{\eta}_x, 1)$  and the unit tangential vector  $\boldsymbol{\tau} = \frac{1}{\sqrt{1+\hat{\eta}_x^2}} (1, \hat{\eta}_x)$ . Then the Neumann boundary condition (2) on the free boundary can be written in the form of

$$-\hat{\eta}_x \hat{\phi}_x + \hat{\phi}_y = 0.$$

This implies that its tangential derivative is also zero, i.e.

$$(\boldsymbol{\tau} \cdot \nabla) (-\hat{\eta}_x \hat{\phi}_x + \hat{\phi}_y) = 0,$$

which is equivalent to

$$-\hat{\eta}_{xx} \hat{\phi}_x - \hat{\eta}_x \hat{\phi}_{xx} + \hat{\phi}_{xy} - \hat{\eta}_x^2 \hat{\phi}_{xy} + \hat{\eta}_x \hat{\phi}_{yy} = 0. \quad (26)$$

Then we have

$$\begin{aligned} \partial_{\mathbf{n}} \left( \left| \nabla \hat{\phi} \right|^2 \right) &= \frac{1}{\sqrt{1+\hat{\eta}_x^2}} (-\hat{\eta}_x \partial_x + \partial_y) (\hat{\phi}_x^2 + \hat{\phi}_y^2) \\ &= \frac{2}{\sqrt{1+\hat{\eta}_x^2}} \hat{\phi}_x (-\hat{\eta}_x \hat{\phi}_{xx} - \hat{\eta}_x^2 \hat{\phi}_{xy} + \hat{\phi}_{xy} + \hat{\eta}_x \hat{\phi}_{yy}) \\ &= \frac{2}{\sqrt{1+\hat{\eta}_x^2}} \hat{\eta}_{xx} (\hat{\phi}_x)^2 \\ &= 2\kappa \left| \nabla \hat{\phi} \right|^2, \end{aligned} \quad (27)$$

where  $\kappa = \partial_x \left( \frac{\hat{\eta}_x}{\sqrt{1+\hat{\eta}_x^2}} \right)$ . The second and last steps are obtained by substituting the Neumann condition, and the third step is obtained by substitution of (26).

On substitution from (27) into (25), the approximate shape linearisation is

$$\left\langle \partial_{\theta} \mathcal{R}_2 \left( \left( \hat{\theta}, \hat{\phi} \right); v \right), \delta \theta \right\rangle \approx \int_{\hat{\Gamma}} \left( 2a\kappa \left| \nabla \hat{\phi} \right|^2 + b n_y \right) w \delta \theta \cdot \mathbf{n} d\Gamma. \quad (28)$$

## 6 Newton-Like Schemes

Now, we introduce  $\phi = \hat{\phi} + \delta\phi$  and  $\theta = \hat{\theta} + \delta\theta \in \Gamma_F$  where  $\delta\phi$  and  $\delta\theta$  are the corrections evaluated in the reference domain  $\hat{\Omega}$ . The exact Newton method for  $(\delta\theta, \delta\phi)$  would be

$$\left\langle \partial_{(\theta, \phi)} \mathcal{R}_1 \left( \left( \hat{\theta}, \hat{\phi} \right); v \right), (\delta\theta, \delta\phi) \right\rangle = -\mathcal{R}_1 \left( \left( \hat{\theta}, \hat{\phi} \right); v \right) \quad \forall v \in V, \quad (29)$$

$$\left\langle \partial_{(\theta, \phi)} \mathcal{R}_2 \left( \left( \hat{\theta}, \hat{\phi} \right); w \right), (\delta\theta, \delta\phi) \right\rangle = -\mathcal{R}_2 \left( \left( \hat{\theta}, \hat{\phi} \right); v \right) \quad \forall w \in W. \quad (30)$$

The Newton-like scheme for  $\mathcal{R}_1$  is obtained by combining (14) and the approximation (17) of  $\partial_{\theta} \mathcal{R}_1 \left( \left( \hat{\theta}, \hat{\phi} \right); v \right)$ , i.e.

$$\int_{\hat{\Omega}} \nabla \delta\phi \cdot \nabla v d\Omega - \int_{\hat{\Gamma}} \text{div}_{\Gamma} \left( \delta\theta \cdot \mathbf{n} \nabla \hat{\phi} \right) v d\Omega - \int_{\hat{\Gamma}} f v \delta\theta \cdot \mathbf{n} d\Gamma = -\mathcal{R}_1 \left( \left( \hat{\theta}, \hat{\phi} \right); v \right), \quad \forall v \in V. \quad (31)$$

1. Initialize with  $(\boldsymbol{\theta}^0, \phi^0)$ ; set  $k = 0$ .
2. Given  $(\boldsymbol{\theta}^k, \phi^k)$ , solve the free boundary problem (34)-(36) with (37) (or(38)) for  $(\delta\boldsymbol{\theta} \cdot \mathbf{n}, \delta\phi)$ .
3. Update the free boundary displacement as

$$\boldsymbol{\theta}^{k+1} = \boldsymbol{\theta}^k + (\delta\boldsymbol{\theta} \cdot \mathbf{n}) \mathbf{m}^k.$$

and  $\phi^k$  as

$$\phi^{k+1} = \phi^k + \delta\phi,$$

with  $\mathbf{m}^k \cdot \mathbf{n} = 1$  on  $\hat{\Gamma}$ . Then repeat from step 2. until convergence.

Table 1: The coupled shape-Newton scheme solving for  $(\delta\boldsymbol{\theta}, \delta\phi)$ .

Similarly, for the Dirichlet boundary condition, the Newton-like scheme is derived based on (19) and approximation (21) as

$$\int_{\hat{\Gamma}} \delta\phi w d\Gamma - \int_{\hat{\Gamma}} (\partial_{\mathbf{n}} h) w \delta\boldsymbol{\theta} \cdot \mathbf{n} d\Gamma = -\mathcal{R}_2 \left( (\hat{\boldsymbol{\theta}}, \hat{\phi}); w \right), \quad \forall w \in W. \quad (32)$$

For the Bernoulli condition, introducing (23) and (28), the Newton-like scheme would be

$$\int_{\hat{\Gamma}} 2a \nabla \hat{\phi} \cdot \nabla \delta\phi w d\Gamma + \int_{\hat{\Gamma}} \left( 2a\kappa |\nabla \hat{\phi}|^2 + b n_y \right) w \delta\boldsymbol{\theta} \cdot \mathbf{n} d\Gamma = -\mathcal{R}_2 \left( (\hat{\boldsymbol{\theta}}, \hat{\phi}); w \right), \quad \forall w \in W. \quad (33)$$

When  $\hat{\phi}$  and  $\hat{\boldsymbol{\theta}}$  are the exact solutions, the approximations are the same as the exact Newton scheme.

The boundary-value problem for  $(\delta\boldsymbol{\theta}, \delta\phi)$  can be extracted based on the Newton-like scheme (31)-(33)

$$\nabla^2 \delta\phi = -\nabla^2 \hat{\phi} - f \quad \text{in } \Omega, \quad (34)$$

$$\partial_{\mathbf{n}} \delta\phi + \text{div}_{\Gamma} \left( \delta\boldsymbol{\theta} \cdot \mathbf{n} \nabla \hat{\phi} \right) - f \delta\boldsymbol{\theta} \cdot \mathbf{n} = 0, \quad \text{on } \hat{\Gamma}, \quad (35)$$

$$\partial_{\mathbf{n}} \delta\phi + \omega \delta\phi = g + \omega h - \left( \partial_{\mathbf{n}} \hat{\phi} + \omega \hat{\phi} \right) \quad \text{on } \Gamma_R, \quad (36)$$

with the boundary condition on the free boundary as either the Dirichlet condition

$$\delta\phi - \partial_{\mathbf{n}} h \delta\boldsymbol{\theta} \cdot \mathbf{n} = h - \phi, \quad \text{on } \hat{\Gamma} \quad (37)$$

or the Bernoulli condition

$$2a \nabla \hat{\phi} \cdot \nabla \delta\phi + \left( 2a\kappa |\nabla \hat{\phi}|^2 + b n_y \right) \delta\boldsymbol{\theta} \cdot \mathbf{n} = - \left( a |\nabla \hat{\phi}|^2 + b \hat{\eta} + c \right), \quad \text{on } \hat{\Gamma}. \quad (38)$$

The algorithm is given in Table 1. The free boundary is updated along the direction of  $\mathbf{m}^k$  with  $\mathbf{m}^k \cdot \mathbf{n} = 1$  such that the free surface can be piecewise smooth. Choosing  $\mathbf{m}^k = \left( 0, \frac{1}{n_y} \right)$ , the free boundary would be updated in the  $y$  direction.

Alternatively, we have  $d\Gamma = ds = \sqrt{1 + \hat{\eta}_x^2} dx$  such that

$$\int_{\hat{\Gamma}} (\cdot) \delta\boldsymbol{\theta} \cdot \mathbf{n} d\Gamma = \int_{\hat{\Gamma}} (\cdot) \delta\eta dx, \quad (39)$$

where  $s$  is the arc length and  $\delta\eta = \sqrt{1 + \hat{\eta}_x^2} (\delta\boldsymbol{\theta} \cdot \mathbf{n}) = \delta\boldsymbol{\theta} \cdot (-\hat{\eta}_x, 1)$ . The boundary integrals can be evaluated in a referenced domain along the  $x$  direction, and this problem can be solved in terms of the pair  $(\delta\eta, \delta\phi)$ . The algorithm is now displayed as Table 2, and the geometry is updated vertically with  $\delta\eta$ .

1. Initialize with  $(\eta^0, \phi^0)$ ; set  $k = 0$ .
2. Given  $(\eta^k, \phi^k)$ , solve the free boundary problem (34)-(36) with (38) for  $(\delta\eta, \delta\phi)$ .
3. Update the free boundary displacement as
$$\eta^{k+1} = \eta^k + \delta\eta.$$
and  $\phi^k$  as
$$\phi^{k+1} = \phi^k + \delta\phi,$$
repeat from step 2. until convergence.

Table 2: The coupled shape-Newton scheme for  $(\delta\eta, \delta\phi)$ .

## 7 Numerical experiments

We start with a straightforward test case for the Dirichlet boundary condition problem and then focus on the submerged triangle problem. The first test case is also a Bernoulli free-boundary problem simplified from the submerged triangle problem, with a Dirichlet condition on both the fixed and free boundary. The submerged triangle problem is the problem to which we are mainly interested in applying this shape-Newton scheme. We will use the algorithm in Table 2 such that the displacement of the free boundary is updated vertically.

### 7.1 Dirichlet boundary condition

The test case for the free-boundary problem with Dirichlet boundary condition is a Bernoulli free-boundary problem derived from a manufactured solution,

$$\phi = x + y, \quad \eta = x + 1, \quad (40)$$

such that the data can be obtained as

$$\begin{aligned} f &= 0, \\ g &= 0, \\ h &= \begin{cases} 2y - 1, & \text{on } \Gamma_F, \\ x + y, & \text{on } \partial\Omega \setminus \Gamma_F. \end{cases} \end{aligned}$$

With an initial domain  $\Omega_0 = \{(x, y) : x \in [0, 1], y \in [0, x^2 + 1]\}$ , how the domain and the triangulation changes in the first three iterations are shown in Figure 2. Starting with a parabola, the free boundary is almost a straight line after the third iteration.

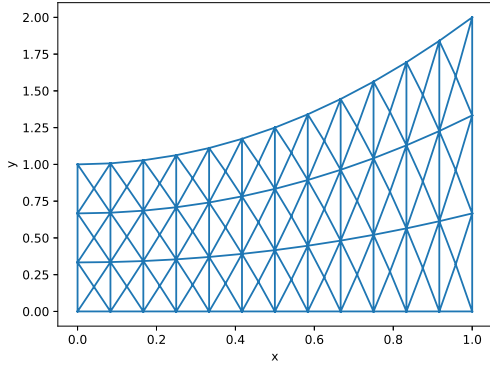
Figure 3 shows the error between numerical results of  $\phi$  and  $\eta$  compared with the exact solution (40) on the free boundary  $\Gamma_F$  with a different number of finite element meshes. The value of  $N + 1$  represents the number of nodes along the  $x$ -axis, and the number of nodes along the  $y$ -axis is  $\frac{N}{4}$ . Although the error is slightly larger with more nodes, the shape-Newton scheme converges superlinearly. Moreover, there appears to be a plateau at higher iterations. One possible reason for the plateau and the rising error values is that we use a finite difference method to find the derivatives and the normal vector. However, even though the error rises with more elements, it is still around  $10^{-12}$  when we choose  $N = 640$  such that there are 409600 elements in total in the domain.

### 7.2 The submerged triangle problem

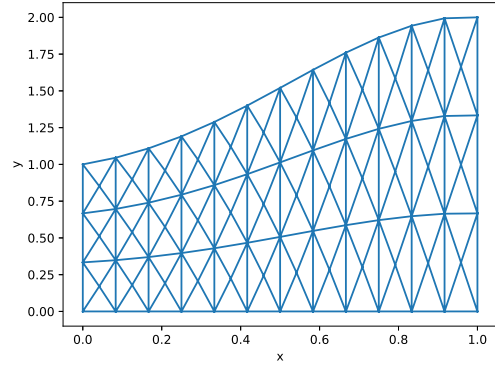
The second test case is the submerged triangle problem investigated by Dias and Vanden-Broeck [18]. A detailed derivation of the governing equations can be found in Appendix A. In this problem, we have a Neumann boundary condition on  $\partial\Omega \setminus \Gamma_R$  and a Dirichlet boundary condition on  $\Gamma_R$ , i.e.  $\omega = 0$  on  $\partial\Omega \setminus \Gamma_R$  and  $\omega \rightarrow \infty$  on  $\Gamma_R$ . The data defining this problem is given as follows:

$$\begin{aligned} f &= 0, \\ g &= \begin{cases} 0, & \text{on } \partial\Omega \setminus \Gamma_L, \\ -1, & \text{on } \Gamma_L, \end{cases} \\ h &= 0 \quad \text{on } \Gamma_R. \end{aligned}$$

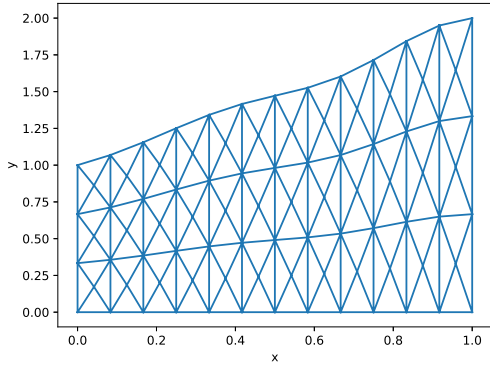




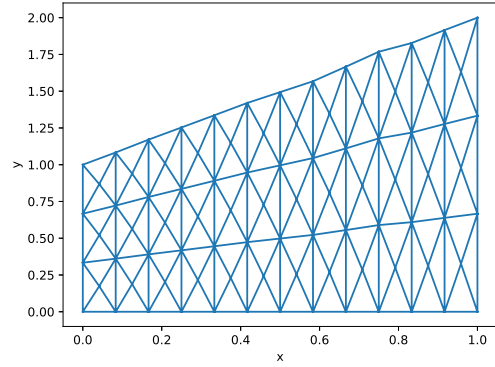
(a) The initial domain and the triangulation.



(b) The domain and the triangulation after the first iteration.



(c) The domain and the triangulation after the second iteration.



(d) The domain and the triangulation after the third iteration.

Figure 2: The initial domain and the change of the domain in three following Newton-like iterations. The free surface is updated vertically.

The Bernoulli condition is obtained by giving  $a = \frac{1}{2}F^2$ ,  $b = 1$  and  $c = \frac{1}{2}F^2 + 1$  where  $F$  is the Froude number. The domain is a rectangle truncated at  $|x| = 4$  containing an isosceles triangle symmetric about  $x = 0$  having an angle  $\alpha$  and width  $2w_0$  at the bottom, as shown in Figure 4. The space is discretised as shown in Figure 5, where it was uniformly spaced along the  $x$ -axis and the vertical direction for fixed values of  $x$ . Then the algorithm in Table 2 can be applied to solve for the pair  $(\delta\eta, \delta\phi)$ , and the free boundary can be updated vertically with  $\delta\eta$ .

Dias and Vanden-Broeck [18] found that the solutions to the submerged problem have two types: One is supercritical flow both upstream and downstream, and the other is supercritical (or subcritical) upstream and subcritical (or supercritical) downstream flow. Our numerical solutions are the first type, and we can compare them with the results in [18].

Some converged grids of the whole region are shown in Figure 6. We noticed that  $\eta(x)$  has a maximum value  $y_0$  at  $x = 0$  on the free boundary, and the value of  $y_0$  can change with the values of  $\alpha$ ,  $w_0$  and  $F$ . Figure 7 shows the value of  $y_0$  against the Froude number  $F$  for various values of  $\alpha$ . We can observe from Figure 7 that  $y_0$  will decrease when the Froude number  $F$  becomes larger for the fixed width of the triangle. In addition, for fixed values of  $F$  and angle  $\alpha$ ,  $y_0$  will also decrease with the width of the triangle. This agrees with the results presented by Dias and Vanden-Broeck in [18], who solved this problem for fixed  $\alpha = \frac{\pi}{4}$ . However, as shown in Figure 7c and Figure 7d, it is hard for us to solve this problem with a larger triangle. This also explains why the critical values obtained from our algorithm are different from the results in [18]. The detail about Dias and Vanden-Broeck's results will be illustrated in Appendix A.

We also found that the solutions are challenging for larger angle  $\alpha$  for fixed width. The possible reason is that with a higher triangle height, the flow can approach its limiting configuration as a thin layer over the edge of the triangle with a stagnation point.

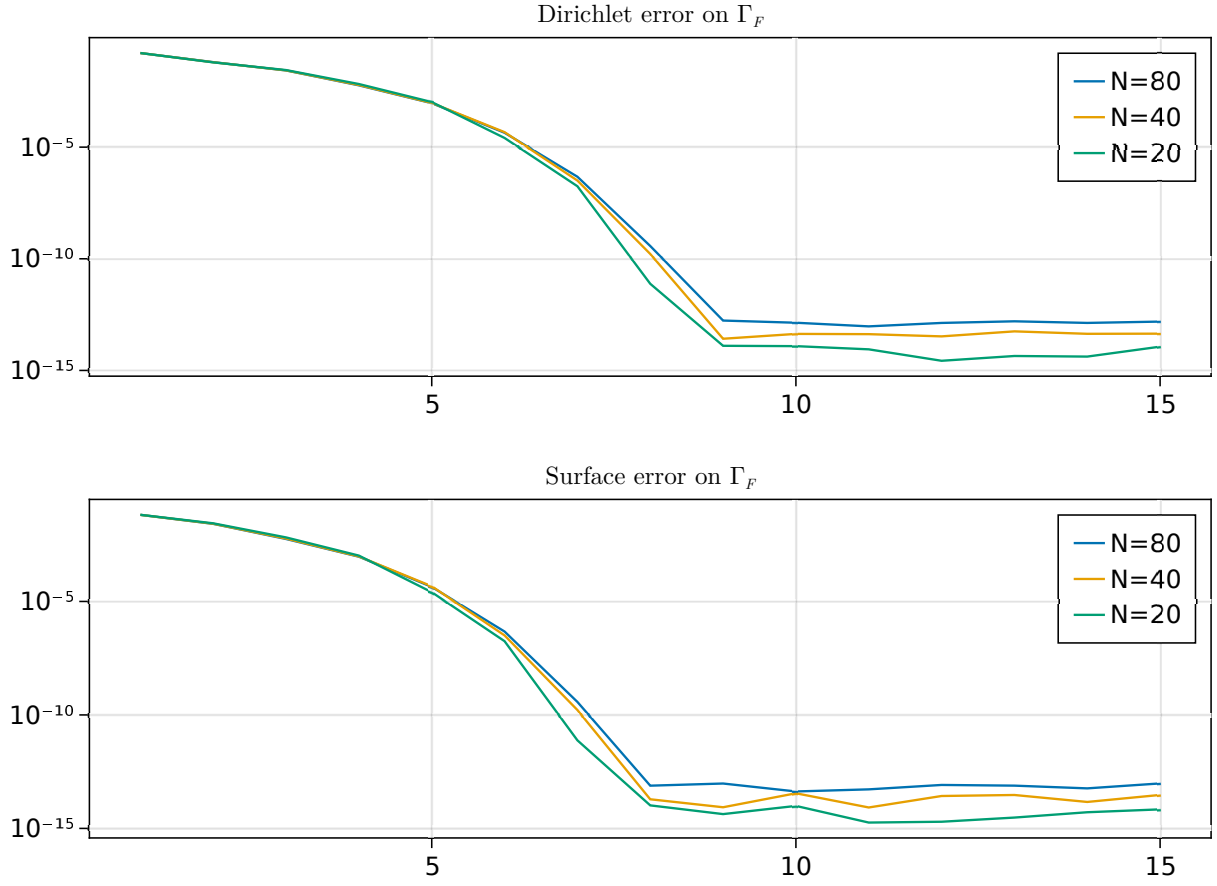


Figure 3: The Dirichlet error  $\|\phi - h\|_{L_\infty}$  and surface error  $\|\eta - \hat{\eta}\|_{L_\infty}$  on  $\Gamma_F$  measured in  $L_\infty$ -form against the number of iterations. The upper plot shows the Dirichlet error, and the lower shows the surface error. The values of  $N + 1$  are the number of the nodes along the  $x$ -axis.

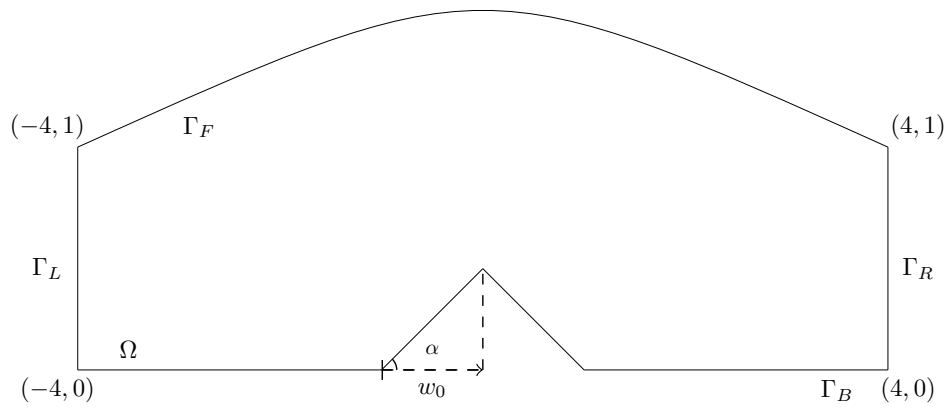


Figure 4: The sketch of the domain we used for the second test case.  $\alpha$  is denoted as the angle and  $w_0$  as the half width of the triangle.

The rate of convergence is shown in Figure 8, where we show the error  $\|\delta\phi\|_{L_2}$  and the surface error  $\|\delta\eta\|_{L_2}$  against the number of iterations for  $\alpha = \frac{\pi}{8}$ ,  $w_0 = 0.3$  and  $F = 3$ . The Dirichlet error  $\delta\phi$  in  $\Omega$  and the surface error  $\delta\eta$  on  $\Gamma_F$  show superlinear convergence. This figure also shows the comparison of the errors for different mesh densities.

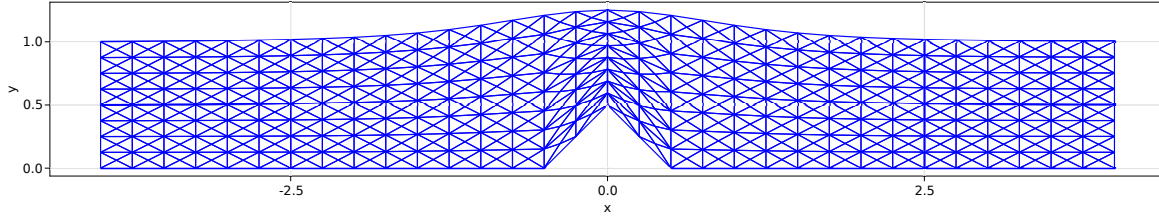


Figure 5: An example of the domain and the triangulation with  $\alpha = \frac{\pi}{4}$ ,  $F = 2$  and the half width of the triangle  $w_0 = 0.5$ .

The Dirichlet error is slightly larger with higher mesh densities but converges faster. The convergence of surface error does not have much difference at the beginning but then has lower values for higher mesh densities. The interesting behaviour is that both the Dirichlet and the surface errors oscillate around some values between order  $10^{-10}$  and  $10^{-13}$ . The order of that values is higher for higher mesh densities, which the discretization error can explain. The convergence is slower as the error becomes very close to the discretization error. In addition, the convergence of surface error slows first, which further affects the Dirichlet error as a consequence of solving as a pair.

## 8 Conclusion

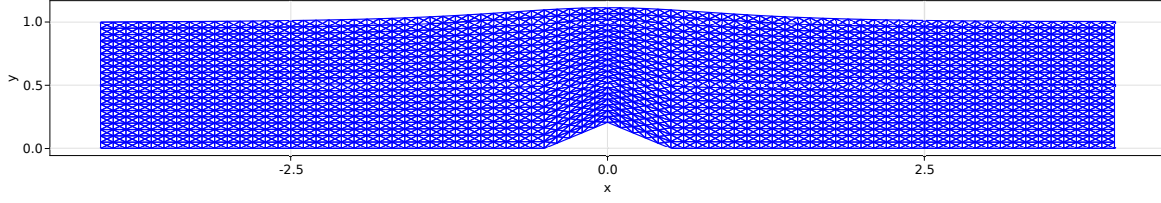
We derived a shape-Newton method to solve generic free-boundary problems. The linearised problems are obtained by applying the Hadamard formula for shape derivatives to the two sets of weak forms of the free boundary problem. After the linearisation and neglecting the small-valued terms, the linearised problem can be solved by a Newton-like scheme with an approximated Jacobian matrix.

The linearisation for the problem with the Dirichlet boundary condition is relatively standard, and we use a straightforward numerical experiment with a manufactured solution to test the numerical schemes. The results agree well with the exact solutions and converge superlinearly.

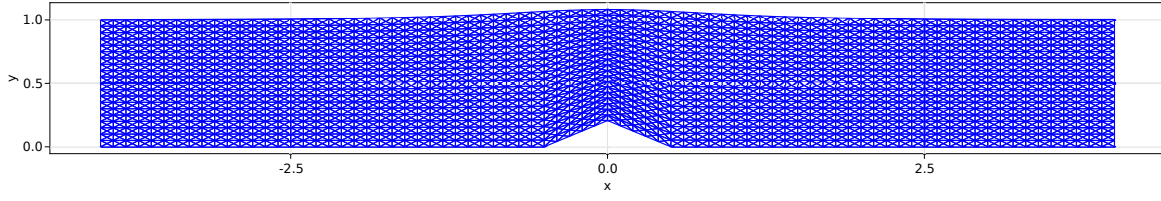
The linearisation for the problem with the Bernoulli equation is interesting. The curvature terms of the shape derivative of the boundary integral can be neglected due to the Neumann boundary condition (2), and only the normal derivative terms remain. However, after some calculations, we find that the normal derivative term satisfies  $\partial_n |\phi|^2 = 2\kappa |\nabla \phi|^2$ . The test problem considers the flow over the submerged triangle problem, whose detail is shown in Appendix A. This chapter only assumes that the inflow and outflow have the same depth and speed. The results in [18] show that for the fixed shape of the triangle, the Froude number  $F$  first decreases and then increases when the maximum deviation of the free boundary increases. This indicates that for some values of  $F$ , two solutions exist. However, our method can only find the solution with the lower maximum deviation due to the limitation of solving the problem with a larger triangle. Despite this, both numerical tests show that the shape-Newton method converges superlinearly.

## References

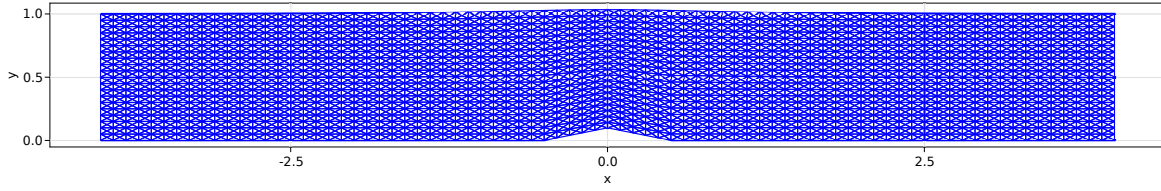
- [1] J. Crank. *Free and Moving Boundary Problems*. Oxford science publications. Clarendon Press, 1987.
- [2] M. Rumpf and M. Flucher. Bernoulli’s free-boundary problem, qualitative theory and numerical approximation. *Journal für die reine und angewandte Mathematik*, 1997(486):165–204, 1997.
- [3] F. Bouchon, S. Clain, and R. Touzani. Numerical solution of the free boundary bernoulli problem using a level set formulation. *Computer methods in applied mechanics and engineering*, 194(36-38):3934–3948, 2005.
- [4] C. M. Kuster, P. A. Gremaud, and R. Touzani. Fast numerical methods for bernoulli free boundary problems. *SIAM journal on scientific computing*, 29(2):622–634, 2007.
- [5] K. Eppler and H. Harbrecht. Efficient treatment of stationary free boundary problems. *Applied numerical mathematics*, 56(10-11):1326–1339, 2006.
- [6] J. Haslinger, K.-H. Hoffmann, and R. A. E. Mäkinen. *Optimal control, dual approach for the numerical solution of a dam problem*. Inst. für Angewandte Mathematik und Statistik, Techn. Univ. München, 1992.



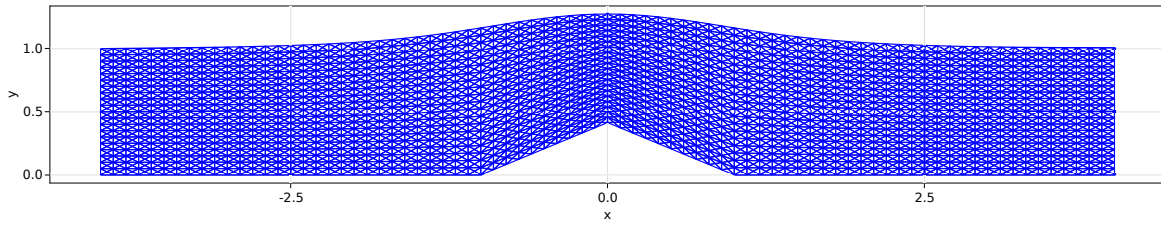
(a) The final domain for  $\alpha = \frac{\pi}{8}$ ,  $w_0 = 0.5$ , and  $F = 1.4$ .



(b) The final domain for  $\alpha = \frac{\pi}{8}$ ,  $w_0 = 0.5$ , and  $F = 2$ .



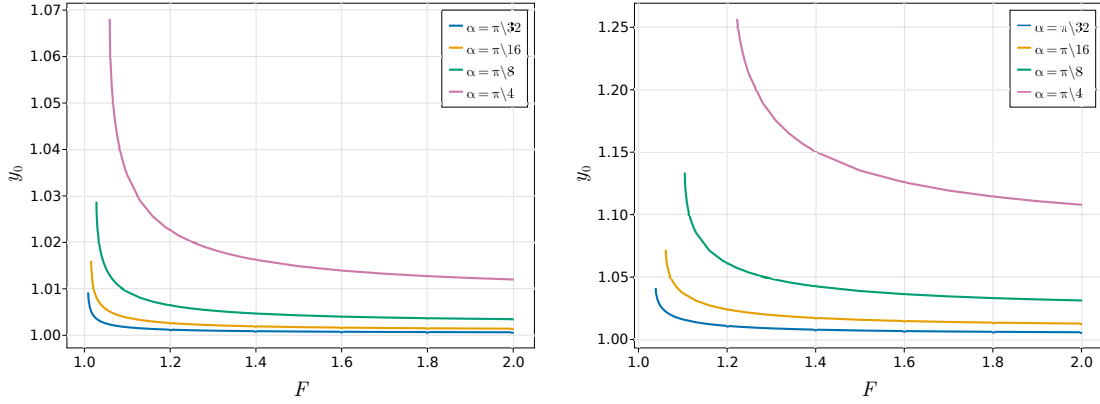
(c) The final domain for  $\alpha = \frac{\pi}{16}$ ,  $w_0 = 0.5$ , and  $F = 2$ .



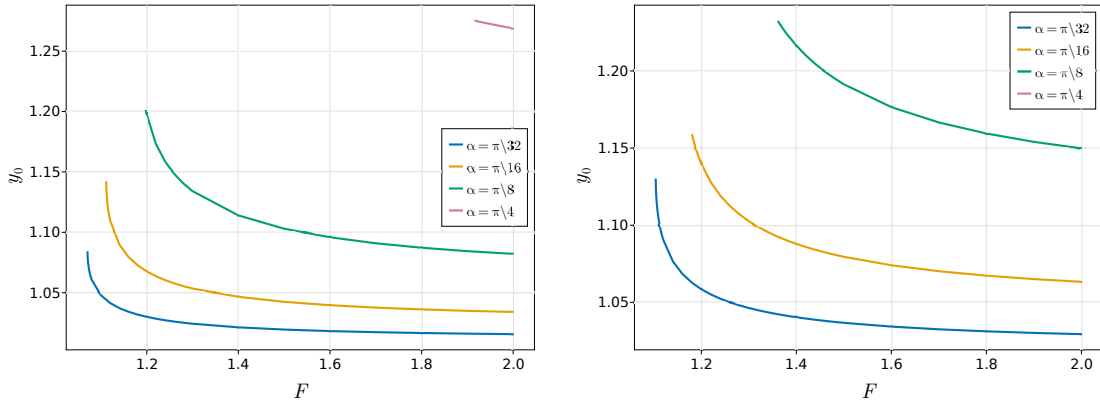
(d) The final domain for  $\alpha = \frac{\pi}{8}$ ,  $w_0 = 1$ , and  $F = 2$ .

Figure 6: The final domains for various  $\alpha$ ,  $w_0$  and  $F$ , where their free boundaries are the numerical solutions.

- [7] J. T. Haslinger, K. Kunisch, and G. Peichl. Shape optimization and fictitious domain approach for solving free boundary problems of bernoulli type. *Computational Optimization and Applications*, 26(3):231–251, 2003.
- [8] T. Tiihonen. Shape optimization and trial methods for free boundary problems. *ESAIM: Mathematical Modelling and Numerical Analysis*, 31(7):805–825, 1997.
- [9] J. I. Toivanen, J. Haslinger, and R. A. E. Mäkinen. Shape optimization of systems governed by bernoulli free



(a) The maximum value  $y$  on the free boundary at  $x = 0$  against  $F$  with  $w_0 = 0.1$  for different values of  $\alpha$ .  
(b) The maximum value  $y$  on the free boundary at  $x = 0$  against  $F$  with  $w_0 = 0.3$  for different values of  $\alpha$ .



(c) The maximum value  $y$  on the free boundary at  $x = 0$  against  $F$  with  $w_0 = 0.5$  for different values of  $\alpha$ .  
(d) The maximum value  $y$  on the free boundary at  $x = 0$  against  $F$  with  $w_0 = 0.7$  for different values of  $\alpha$ .

Figure 7: The maximum value  $y_0$  on the free boundary at  $x = 0$  against  $F$  for different values of  $\alpha$  and  $w_0$ .

- boundary problems. *Computer Methods in Applied Mechanics and Engineering*, 197(45-48):3803–3815, 2008.
- [10] E. H. Van Brummelen and A. Segal. Numerical solution of steady free-surface flows by the adjoint optimal shape design method. *International Journal for Numerical Methods in Fluids*, 41(1):3–27, 2003.
- [11] G. Mejak. Numerical solution of bernoulli-type free boundary value problems by variable domain method. *International journal for numerical methods in engineering*, 37(24):4219–4245, 1994.
- [12] K.G. van der Zee, E.H. van Brummelen, I. Akkerman, and R. de Borst. Goal-oriented error estimation and adaptivity for fluid–structure interaction using exact linearized adjoints. *Computer Methods in Applied Mechanics and Engineering*, 200(37):2738–2757, 2011. Special Issue on Modeling Error Estimation and Adaptive Modeling.
- [13] M. Delfour and J.-P. Zolésio. *Shapes and Geometries: Analysis, Differential Calculus and Optimization*, volume 4. 01 2001.
- [14] J. Sokolowski and J.-P. Zolésio. *Introduction to shape optimization: shape sensitivity analysis*. Springer Series in Computational Mathematics. Springer, Berlin, Heidelberg, 1992.
- [15] K. T. Kärkkäinen and T. Tiihonen. Shape calculus and free boundary problems. In *Proceedings of the European Congress on Computational Methods in Applied Sciences and Engineering, ECCOMAS*, 2004.
- [16] K. T. Kärkkäinen and T. Tiihonen. Free surfaces: shape sensitivity analysis and numerical methods. *International Journal for Numerical Methods in Engineering*, 44(8):1079–1098, 1999.
- [17] K. G. van der Zee, G. J. van Zwieten, C. V. Verhoosel, and E. H. van Brummelen. Shape-newton method for isogeometric discretizations of free-boundary problems. In *MARINE 2011, IV International Conference on Computational Methods in Marine Engineering*, pages 85–102. Springer, 2013.

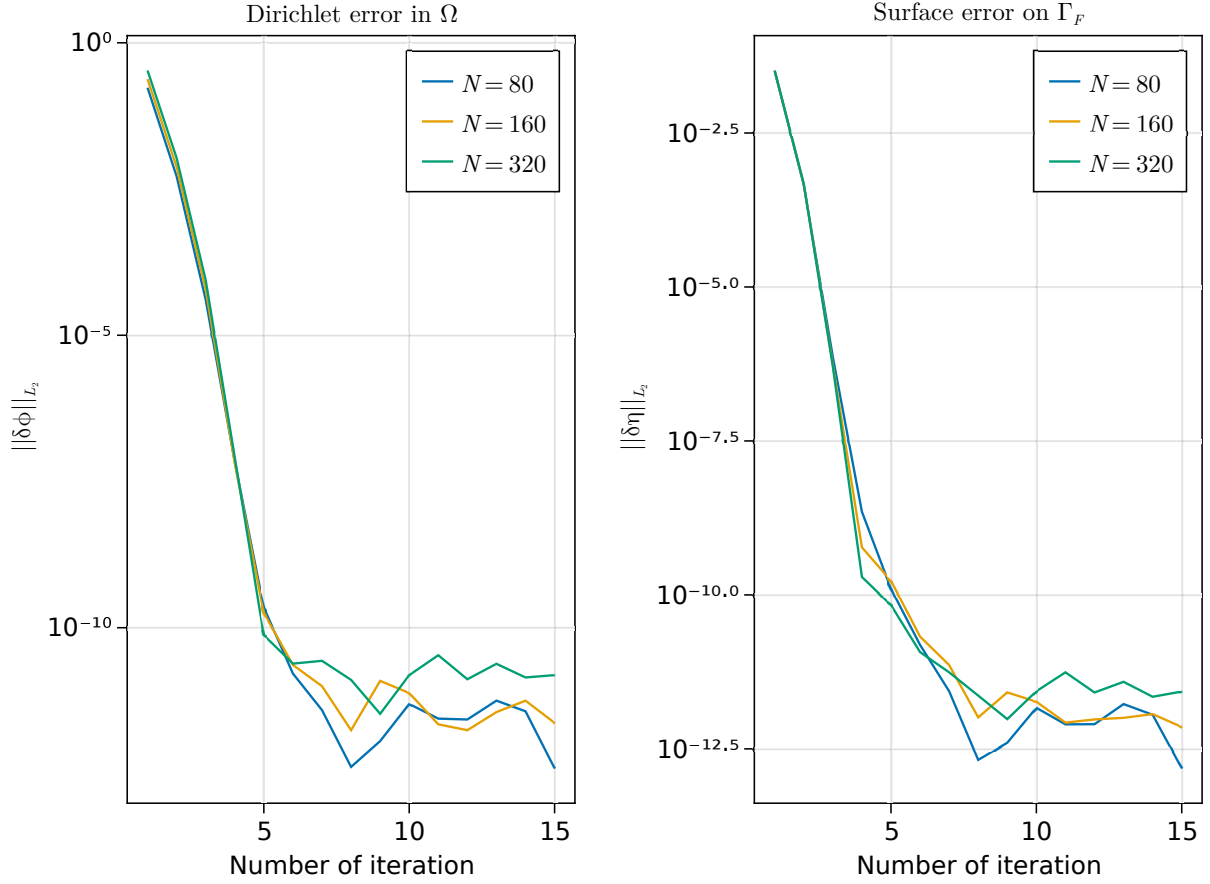


Figure 8: The error  $\|\delta\phi\|_{L_2}$  and surface error  $\|\delta\eta\|_{L_2}$  on  $\Gamma_F$  measured in  $L_\infty$ -form against the number of iterations with  $\alpha = \frac{\pi}{8}$ ,  $w_0 = 0.3$  and  $F = 3$ . The upper plot shows the Dirichlet error, and the lower shows the surface error. The values of  $N + 1$  are the number of the nodes along the  $x$ -axis.

- [18] F. Dias and J.-M. Vanden-Broeck. Open channel flows with submerged obstructions. *Journal of Fluid Mechanics*, 206:155–170, 1989.

## A Submerged Triangle Problem

The submerged triangle problem is from [18], and we will give the detail about how Dias and Vanden-Broeck formulate this problem. The model considers a steady irrotational flow of an incompressible, inviscid fluid over a triangular obstruction as shown in Fig.9a. A system of Cartesian coordinates is introduced, where the  $x$ -axis is along the parallel bottom plate and the  $y$ -axis going through the apex (point  $B$ ) of the triangle. The acceleration of gravity  $g$  acts in the negative  $y$ -direction. The flow approaches a uniform stream when  $|x| \rightarrow \infty$ , where the upstream flow has velocity  $U$  and depth  $L$ , and the downstream flow has velocity  $\tilde{U}$  and depth  $\tilde{L}$ . The height of the triangle is denoted as  $W$ . We introduce the velocity potential of this flow as  $\phi(x, y)$  and the location of the free surface  $y(x)$ . The Froude number  $F$  is defined as

$$F = \frac{U}{(gL)^{\frac{1}{2}}}. \quad (41)$$

Now we introduce dimensionless variables

$$x' = \frac{x}{L}, \quad y' = \frac{y}{L}, \quad \phi' = \frac{\phi}{UL}, \quad y' = \frac{y}{L}, \quad \tilde{L}' = \frac{\tilde{L}}{L}, \quad \tilde{U}' = \frac{\tilde{U}}{U}. \quad (42)$$

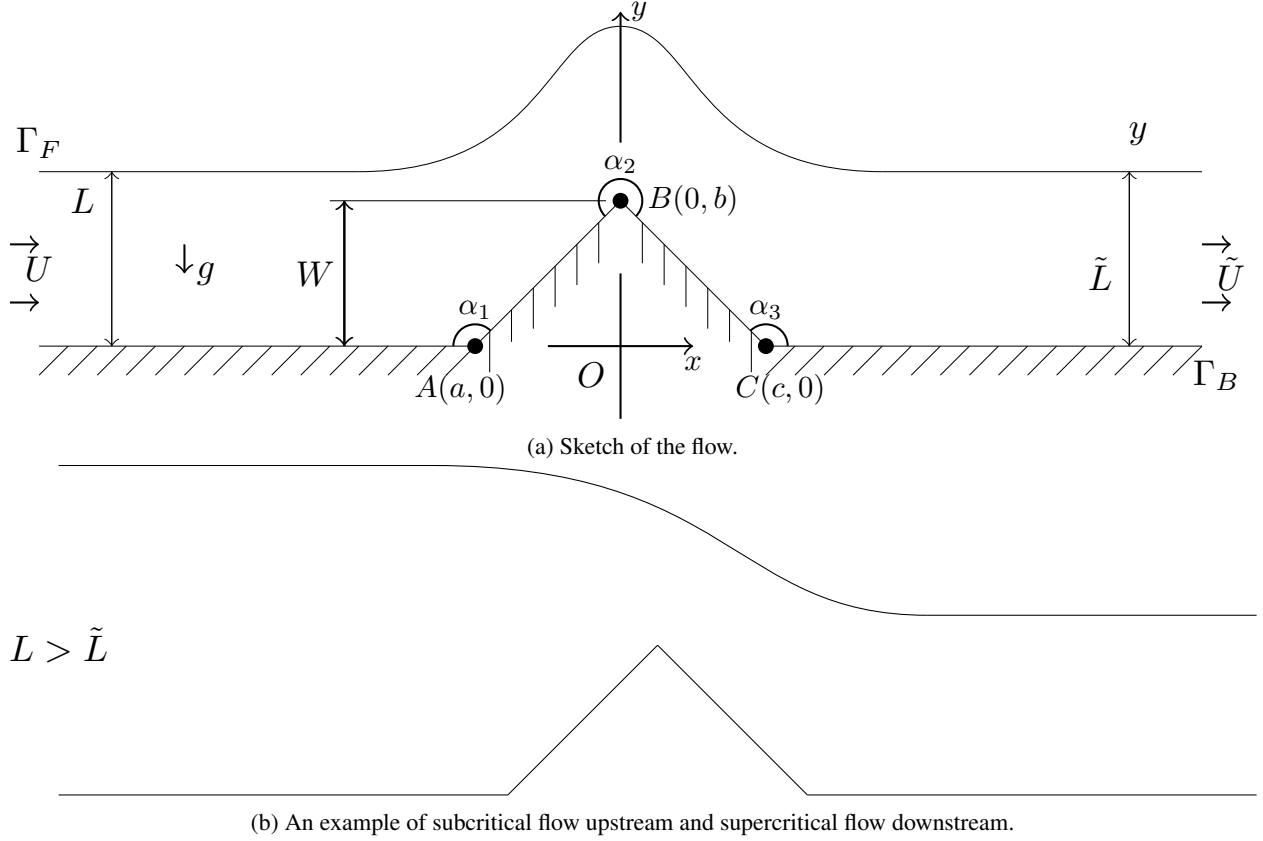


Figure 9: This shows two different types of solutions and the sketch of the flow. 9a is a sketch of the flow for  $U = \tilde{U}$ ,  $L = \tilde{L}$  and  $F \geq 1$ . 9b is an example of subcritical flow upstream and supercritical flow downstream.

We drop primes for convenience of notations. When  $\tilde{L} \leq 1$ , the flow is defined as subcritical upstream and supercritical downstream (as shown in Fig.9b). Moreover, the flow is supercritical upstream and downstream when  $\tilde{L} = 1$  and  $F \geq 1$ .

We denote the whole region of the flow as  $\Omega$ , the bottom plate as  $\Gamma_B$  and the free surface as  $\Gamma_F$ . The Bernoulli condition on  $\Gamma_F$  is

$$\frac{1}{2}F^2|\nabla\phi|^2 + y = \text{constant}, \quad \text{on } \Gamma_F. \quad (43)$$

The constant value on the right-hand side of the Bernoulli equation can be evaluated by considering the conditions upstream. Then the Bernoulli equation on the free surface is

$$\frac{1}{2}F^2|\nabla\phi|^2 + y = \frac{1}{2}F^2 + 1. \quad (44)$$

Now the governing equation and boundary conditions are

$$\nabla^2\phi = 0, \quad \text{in } \Omega, \quad (45)$$

$$\frac{1}{2}F^2|\nabla\phi|^2 + y = \frac{1}{2}F^2 + 1, \quad \text{on } \Gamma_F, \quad (46)$$

$$\frac{\partial\phi}{\partial\mathbf{n}} = 0, \quad \text{on } \Gamma_F, \quad (47)$$

$$\frac{\partial\phi}{\partial\mathbf{n}} = 0, \quad \text{on } \Gamma_B, \quad (48)$$

$$\phi_x = 1, \quad x \rightarrow -\infty, \quad (49)$$

$$\phi = 0, \quad x \rightarrow -\infty, \quad (50)$$

$$y = 1, \quad x \rightarrow \infty, \quad (51)$$

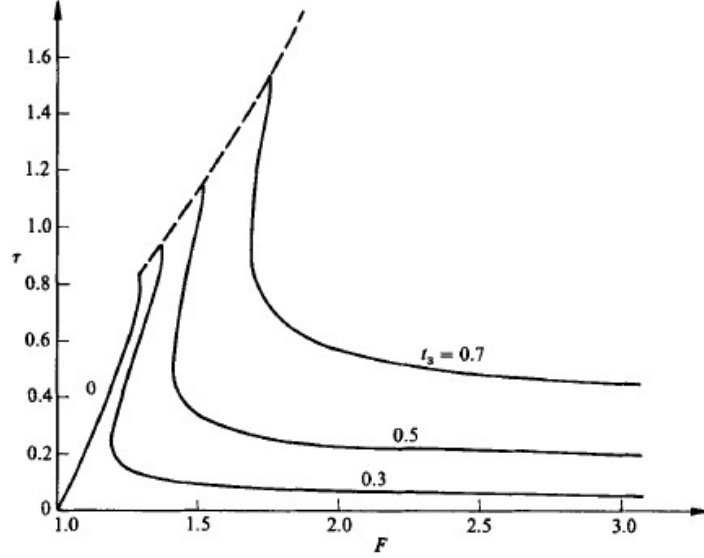


Figure 10:  $\tau$  is the maximum value of the deviation of the free surface.  $t_3$  defines the geometry of the triangle by using conformal mapping and then mapping to a half-unit circle called  $t$ -plane. The dashed line shows the analytical values of the maximum of  $\tau$  with respect to  $F$ . The curve noted 0 is the solitary wave when  $t_4 = 0$ . This graph is from [18].

where  $\mathbf{n}$  is the unit normal to the boundary pointing out the flow.

According to [18], two different types of solutions are derived by considering the Bernoulli condition at  $|x| \rightarrow \infty$  as

$$\frac{1}{2}F^2 + 1 = \frac{1}{2}F^2\tilde{U}^2 + \tilde{L}. \quad (52)$$

The discharge  $Q$  is defined as

$$Q = UL = \tilde{U}\tilde{L}. \quad (53)$$

Then we can eliminate  $\tilde{U}$  in (52) by substituting (53) such that

$$(\tilde{L} - 1) \left[ \frac{1}{2}F^2 \left( \frac{1}{\tilde{L}} + 1 \right) - \tilde{L} \right] = 0. \quad (54)$$

It is obvious that this equation has two solutions :

$$\tilde{L} = 1, \quad (55)$$

and

$$F^2 = \frac{2\tilde{L}^2}{1 + \tilde{L}}. \quad (56)$$

The first solution (55) indicates that  $\tilde{L} = L$  and  $\tilde{U} = U$ . For the solution (56), it can be shown that  $F \geq 1$  when  $\tilde{L} \geq 1$ , and  $F \leq 1$  when  $\tilde{L} \leq 1$ . In [18], when considering the second type of the solutions, Dias and Vanden-Broeck assume that  $\tilde{L} \leq 1$ , thus the flow is subcritical upstream and supercritical downstream. An example of this flow is shown in Fig.9b.

The results we compare are for the first solution for  $F \geq 1$  as shown in Fig.10 [18].  $\tau$  is the maximum value of the deviation of the free surface, which is equivalent to  $y_0$  in our notation.  $t_3$  defines the geometry of the triangle by using conformal mapping and then mapping to a half-unit circle called  $t$ -plane. Dias and Vanden-Broeck found that  $F$  first decrease then increase as  $\tau$  becomes larger, indicating two solutions for some values of  $F$ . By considering the solitary wave, i.e.  $t_3 = 0$ , they found that the maximum of  $\tau$  satisfies  $\tau_{max} = \frac{1}{2}F^2$ .